

NASA/CR-97- 207296

Assessing Aircraft Susceptibility to Nonlinear Aircraft-Pilot Coupling/Pilot-Induced Oscillations

R. A. Hess¹ and P. W. Stout²

Department of Mechanical and Aeronautical Engineering
University of California
Davis, CA 95616

NIS
IN-08-CR
067605

Abstract

A unified approach for assessing aircraft susceptibility to aircraft-pilot coupling (or pilot-induced oscillations) which was previously reported in the literature and applied to linear systems is extended to nonlinear systems, with emphasis upon vehicles with actuator rate saturation. The linear methodology provided a tool for predicting (1) handling qualities levels, (2) pilot-induced oscillation rating levels and (3) a frequency range in which pilot-induced oscillations are likely to occur. The extension to nonlinear systems provides a methodology for predicting the latter two quantities. Eight examples are presented to illustrate the use of the technique. The dearth of experimental flight-test data involving systematic variation and assessment of the effects of actuator rate limits presently prevents a more thorough evaluation of the methodology.

Introduction

An adverse aircraft-pilot coupling (APC) or pilot-induced oscillation (PIO) can be defined as an unwanted, inadvertent and atypical closed-loop coupling between a pilot and the response variables of an aircraft.¹ For the uninitiated reader, a concise historical perspective of the APC/PIO problem can be found in Ref. 2. The importance and serious nature of APC/PIO's in the development of modern aircraft with fly-by-wire (FBW) flight control systems has led NASA to sponsoring a National Research Council (NRC) Committee to study the APC/PIO problem.³ More recent results can be found in the summary of four research efforts sponsored by the Air Force.^{4,5,6,7} Despite continuing research in this area, there has been little consensus about the APC/PIO phenomenon in terms of the pilot behavior that initiates and sustains the oscillation. To help fill this void, the

first author has proposed a unifying theory and methodology for assessing both the handling qualities and the APC/PIO susceptibility of aircraft and flight control systems described by linear dynamics.⁸ Although APC/PIO susceptibility is certainly a handling qualities issue, discussing the two in separate fashion is not unreasonable, given the demonstrable fact that an aircraft can exhibit poor handling qualities and still not be APC/PIO prone. Although the pilot/vehicle modeling procedure to be discussed has been applied to the study of "roll ratchet" (a high-frequency APC/PIO) this phenomenon will not be discussed here. The technique for assessing linear handling qualities and APC/PIO susceptibility is reviewed in the next section and is based upon the work of Ref. 8. A means of extending this methodology to nonlinear systems is then presented. A series of examples demonstrate the use of the methodology in prediction of APC/PIO susceptibility. A brief discussion, a synopsis of the analysis technique, and a statement of conclusions follow.

Overview of a Unified Theory for Handling Qualities and APC/PIO

The methodology for assessing vehicle handling qualities and APC/PIO susceptibility is based upon a revised structural model of the human pilot shown in Fig. 1 and discussed in detail in Refs. 8 and 9. This model has its genesis in an earlier structural model,¹⁰ and in a later modification of that model.¹¹ As shown in Fig. 1, the model describes compensatory pilot behavior, i.e., behavior involving closed-loop tracking in which the visual input is system error. The elements within the dashed box represent the dynamics of the human pilot. The reader is referred to Ref. 8 for a thorough discussion of the model and its parameterization in pilot/vehicle analyses. Only a brief

¹Professor, Associate Fellow AIAA

²Graduate Student, Senior Member AIAA

spectral density of a proprioceptive feedback signal within a structural pilot model, the parameters of which have been selected in a specific manner. Rather than relying upon describing function analyses, the technique employs a computer simulation of the pilot/vehicle system. As such, it is not limited to single, isolated nonlinearities. The APC/PIO frequency for vehicles predicted to have a $PIOR \geq 4$ can be bracketed by: (1) the frequency of the stable limit cycle produced with the minimum error-rate gain in the model when no proprioceptive feedback is being used, and (2) the frequency at which the peak in the scaled power spectral density of the proprioceptive feedback signal in the pilot model occurs when such feedback is being used. As in the case of all such techniques aimed toward the prediction of nonlinear APC/PIO events, an adequate data base needs to be created so the proposed methodology can be evaluated and improved.

Acknowledgement

This research was supported by NASA Langley Research Center under grant No. NAG1-1744. Dr. Barton Bacon was the contract technical manager.

References

- ¹Smith, R. H., "A Theory for Longitudinal Short-Period Pilot Induced Oscillations," Air Force Flight Dynamics Lab., AFFDL-TR-77-57, June 1977.
- ²McRuer, D. T., "Pilot-Induced Oscillations and Human Dynamic Behavior," NASA CR 4683, 1995.
- ³Anon., *Aviation Safety and Pilot Control - Understanding and Preventing Unfavorable Pilot-Vehicle Interactions*, Report of the NRC Committee on the Effects of Aircraft Pilot Coupling on Flight Safety, National Academy Press, Washington, DC, 1997.
- ⁴Klyde, D. H., McRuer, D. T., Myers, T. T., "Unified Pilot-Induced Oscillation Theory, Volume I: PIO Analysis with Linear And Nonlinear Effective Vehicle Characteristics, Including Rate Limiting, Air Force Flight Dynamics Directorate, WL-TR-96-3028, 1995.
- ⁵Preston, J. D., Citurs, K., Hodgkinson, J., Mitchell, D. C., Buckley, J., and Hoh, R. H., "Unified Pilot-Induced Oscillation Theory, Volume II: Pilot-Induced Oscillation Criteria Applied to Several McDonnell Douglas Aircraft, Air Force Flight Dynamics Directorate, WL-TR-96-3029, 1995.
- ⁶Anderson, M. R., and Page, A. B., "Unified Pilot-Induced Oscillation Theory, Volume III: PIO Analysis Using Multivariable Methods," Air Force Flight Dynamics Directorate, WL-TR-96-3030, 1995.
- ⁷Bailey, R. E., and Bidlack T. J., "Unified Pilot-Induced Oscillation Theory, Volume IV: Time-Delay Neal-Smith Criterion, Air Force Flight Dynamics Directorate, WL-TR-96-3031, 1995.
- ⁸Hess, R. A., "A Unified Theory for Aircraft Handling Qualities and Adverse Aircraft-Pilot Coupling, *Journal of Guidance, Control, and Dynamics*, to appear.
- ⁹Hess, R. A., "A Theory for Roll Ratchet Phenomenon in High Performance Aircraft, submitted for consideration for AIAA 1997 Atmospheric Flight Mechanics Conference, August 11-13, 1997, New Orleans, LA.
- ¹⁰Hess, R. A., "A Model for the Human's Use of Motion Cues in Vehicular Control," *Journal of Guidance, Control, and Dynamics*, Vol. 13, No. 3, 1990, pp. 476-482.
- ¹¹Hess, R. A., "Analyzing Manipulator and Feel System Effects in Aircraft Flight Control," *IEEE Transactions on Systems, Man, and Cybernetics*, Vol. 20, No. 4, 1990, pp. 923-931.
- ¹²Hess, R. A., "Feedback Control Models - Manual Control and Tracking," in *Handbook of Human Factors and Ergonomics, 2nd Ed.*, Ed: G. Salvendy, Wiley, New York, 1997, to appear.
- ¹³Dornheim, M. A., "Report Pinpoints Factors Leading to YF-22 Crash," *Aviation Week and Space Technology*, Nov. 9, 1992, pp. 53-54.
- ¹⁴Duda, H., "Prediction of Adverse Aircraft-Pilot Coupling in the Roll Axis due to Rate Limiting in Flight Control Systems," DLR IB 111-96/13, DLR Institut fur Flugmechanik, Braunschweig, March 1996.
- ¹⁵Smith, R. H., "Predicting and Validating Fully-Developed PIO," AIAA Paper 94-3669, August, 1994.
- ¹⁶Golubev, M. and Horowitz, I. M., "Plant Rational Transfer Function Approximation from Input-Output Data," *International Journal of Control*, Vol. 36, pp. 711-723, 1982.
- ¹⁷Anon., "Why the Gripen Crashed," *Aerospace America*, Feb., 1994, p.11.
- ¹⁸Bjorkman, E. A., "Flight Test Evaluation of Techniques to Predict Longitudinal Pilot Induced Oscillations," M. S. Thesis, Air Force Institute of Technology, AFIT/BAE/AA/86J-1, 1986.

Table 1. Vehicle Description for LAHOS Configs. 4-7 and 4-4

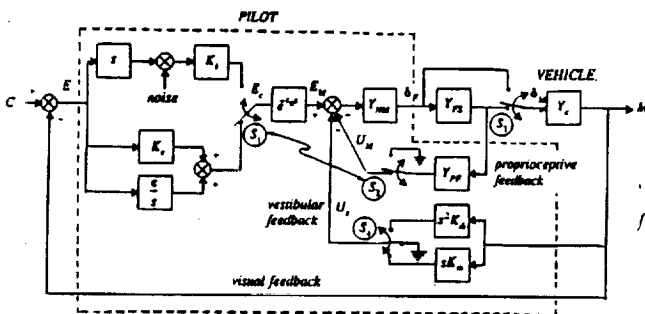
^a time delay added in analysis to degrade vehicle handling qualities

Fig. 1 The revised structural model of the human pilot.

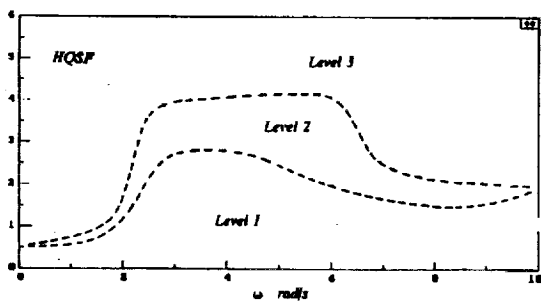


Fig. 2 HQSF bounds from Ref. 8 delineating handling qualities levels.

DESCRIPTION	NUMERICAL RATING
NO TENDENCY FOR PILOT TO INDUCE UNDESIRABLE MOTIONS	1
UNDESIRABLE MOTIONS TEND TO OCCUR WHEN PILOT INITIATES ABRUPT MANEUVERS OR ATTEMPTS TIGHT CONTROL. THESE MOTIONS CAN BE PREVENTED OR ELIMINATED BY PILOT TECHNIQUE	2
UNDESIRABLE MOTIONS EASILY INDUCED WHEN PILOT INITIATES ABRUPT MANEUVERS OR ATTEMPTS TIGHT CONTROL. THESE MOTIONS CAN BE PREVENTED OR ELIMINATED BUT ONLY AT SACRIFICE TO TASK PERFORMANCE OR THROUGH CONSIDERABLE PILOT ATTENTION AND EFFORT	3
OSCILLATIONS TEND TO DEVELOP WHEN PILOT INITIATES ABRUPT MANEUVERS OR ATTEMPTS TIGHT CONTROL. PILOT MUST REDUCE GAIN OR ABANDON TASK TO RECOVER	4
DIVERGENT OSCILLATIONS TEND TO DEVELOP WHEN PILOT INITIATES ABRUPT MANEUVERS OR ATTEMPTS TIGHT CONTROL. PILOT MUST OPEN LOOP BY RELEASING OR FREEZING THE STICK	5
DISTURBANCE OR NORMAL PILOT CONTROL MAY CAUSE DIVERGENT OSCILLATION. PILOT MUST OPEN CONTROL LOOP BY RELEASING OR FREEZING THE STICK	6

Fig. 3 The Pilot-Induced Oscillation Rating (PIOR) scale.

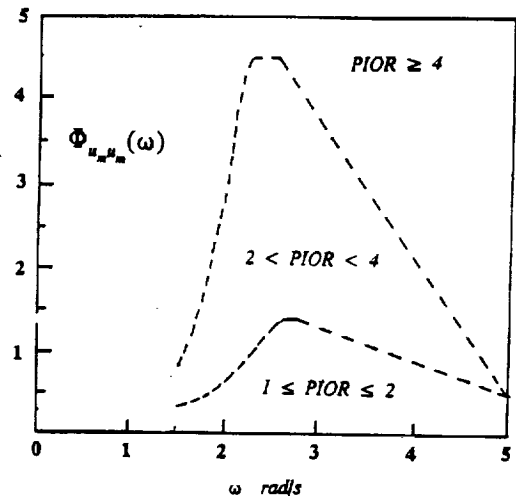


Fig. 4 $\Phi_{\mu, \mu, \mu}(\omega)$ bounds from Ref. 8 delineating PIOR levels.

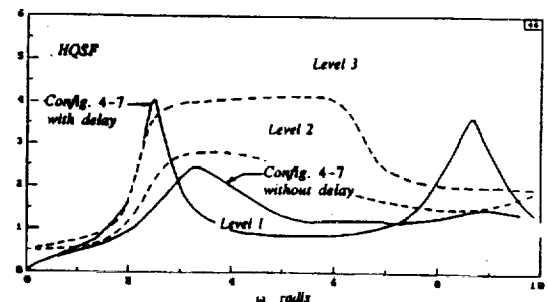


Fig. 5 HQSF for LAHOS Config. 4-7 without and with 0.2 s time delay.

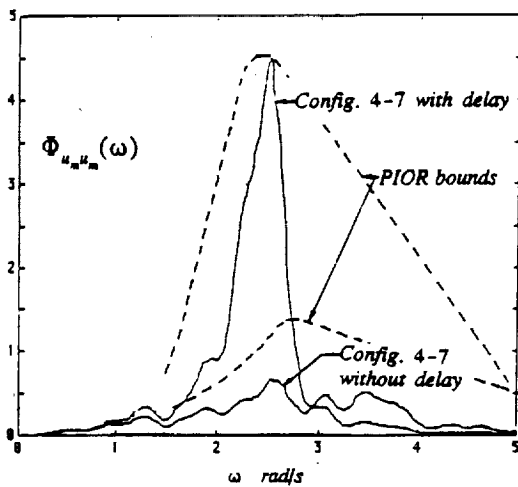


Fig. 6 $\Phi_{u_w u_w}(\omega)$ for LAHOS Config. 4-7 without and with 0.2 s time delay.

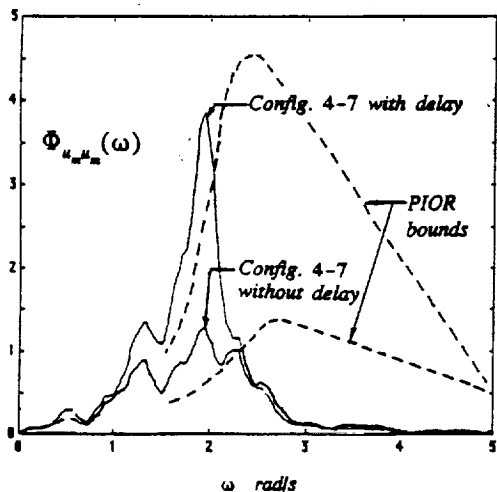


Fig. 7 $\Phi_{u_w u_w}(\omega)$ for LAHOS Config. 4-7 without and with 0.2 s time delay with 25 deg/s actuator rate limiting.

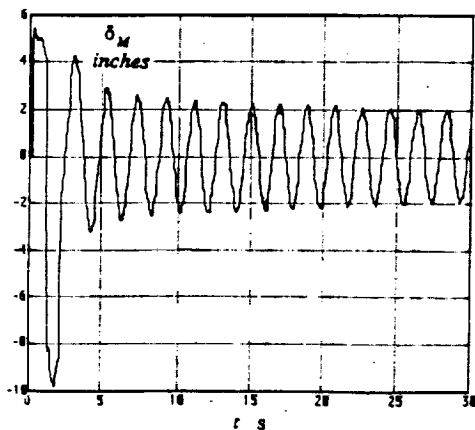


Fig. 8 Stick displacement in simulated pilot/vehicle system for Config. 4-7 with 0.2 s time delay and 25 deg/s actuator rate limiting.

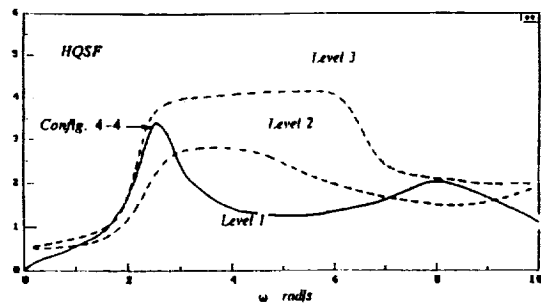


Fig. 9 HQSF for LAHOS Config. 4-4

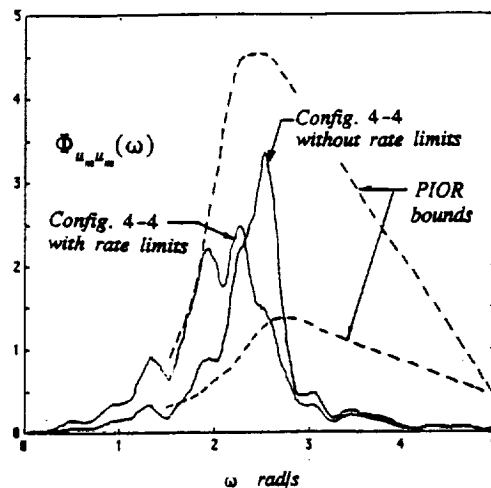


Fig. 10 $\Phi_{u_w u_w}(\omega)$ for LAHOS Config. 4-4 without and with 25 deg/s actuator rate limiting.

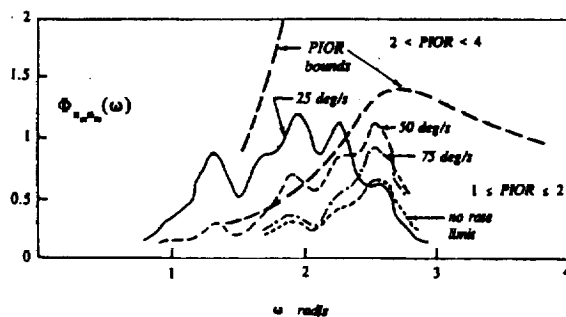


Fig. 11 $\Phi_{u_w u_w}(\omega)$ for LAHOS Config. 4-7 without time delay and with actuator rate limiting of various magnitudes.

overview will be presented here.

Starting from the left in Fig. 1, the system error $e(t)$ follows one of two possible paths. The upper path is intended to model the human's visual rate-sensing dynamics, here modeled by a differentiator (s), and a gain K_e . The lower path describes normal error sensing and gain compensation K_e , including the possibility of the human's accomplishing low-frequency trim (or integral) compensation via e/s . The switch labeled S_1 allows switching between error and error-rate tracking, a critical component of the model in describing the initiation and sustenance of APC/PIO's. A central processing time delay, τ_0 , is also included. The elements Y_{NM} and Y_{PS} are intended to represent, respectively, the open-loop dynamics of the neuromuscular system driving the cockpit inceptor, typically a control stick, and the dynamics of the inceptor force-feel system, itself. The element Y_{PF} and its position in the model is central to the philosophy of the structural model, i.e., the primary equalization capabilities of the human pilot are assumed to occur through operation upon a proprioceptively sensed, as opposed to a visually sensed, variable. Switches S_1 and S_2 are assumed to operate in unison, i.e. when S_1 is "up", so is S_2 . The switch S_3 allows study of control inceptors which drive the vehicle through either *position* or applied *force*. Switch S_4 is hypothesized to play an important role in roll ratchet⁹ and concerns the human's use of vestibular or motion cues. Herein, it will always be in the open position, i.e. no vestibular feedback will be assumed. Vehicle output feedback completes the model.

Pilot model parameter selection is straightforward and is discussed in Ref. 8. Only the results are presented here. Elements Y_{NM} and Y_{PF} are given by

$$Y_{NM} = \frac{\omega_{NM}^2}{s^2 + 2\zeta_{NM}\omega_{NM}s + \omega_{NM}^2} \quad (1)$$

$$Y_{PF} = \begin{cases} K(s+a) & \text{or,} \\ K & \text{or,} \\ K/(s+a) \end{cases} \quad (2)$$

with the particular equalization of Eq. 2 dependent upon

the form of the vehicle dynamics, Y_c , around the crossover frequency. The three forms of Eqs. 2 can be interpreted as the pilot's "internal model" of the vehicle dynamics. That is, in the range of crossover, $Y_{PF} \propto s \cdot Y_c(s)$. For reasons described in Ref. 8, a constant crossover frequency $\omega_c = 2.0 \text{ rad/s}$ is chosen.

As in applications of the original structural model, a number of model parameters in the revised model of Fig. 1 can be considered invariant across different vehicles and tasks. Nominal values of these "fixed" parameters are

$$\begin{aligned} \tau_0 &= 0.2 \text{ s} \\ \omega_{NM} &= 10 \text{ rad/s} \\ \zeta_{NM} &= 0.7 \end{aligned} \quad (3)$$

The relatively simple relations of Eqs. 1-3 and the crossover relation $\omega_c = 2.0 \text{ rad/s}$ are sufficient to implement the model of Fig. 1. One of the three forms on the right hand side of Eq. 2 is selected so that the resulting open loop transfer function is

$$Y_p Y_c = \frac{\delta_M}{E}(j\omega) \cdot Y_c(j\omega) \approx \frac{\omega_c}{j\omega} e^{-\tau_e s} \text{ for } \omega \approx \omega_c \quad (4)$$

i.e., $Y_p Y_c(j\omega)$ follows the dictates of the crossover model of the human pilot.¹² The time delay τ_e in Eq. 4 is an "effective" delay, not to be confused with τ_0 in Fig. 1. It is important to specify precisely how Eq. 4 is employed in the modeling procedure. Limiting discussion to the second and third forms of Y_{PF} (those most likely to be encountered in pilot/vehicle analyses), the right hand side of Eq. 2 is selected so that

$$\left| \frac{K}{Y_{PF}(j\omega)} \cdot Y_c(j\omega) \right| \approx \frac{K_1}{j\omega} \text{ for } \begin{cases} \omega \approx \omega_c \\ K_1 \text{ arbitrary} \end{cases} \quad (5)$$

The gain K appearing in Eqs. 2 and 5 is chosen so that the minimum damping ratio of any quadratic closed-

loop poles of $\frac{\delta_M}{E_M}(s)$ is $\zeta_{\min} = 0.15$ when all other loops are open. Finally, K_e is selected so that the desired crossover frequency of 2.0 rad/s is obtained.

The handling qualities assessment technique discussed in Ref. 8 defines a *Handling Qualities Sensitivity Function* (HQSF) as

$$HQSF \propto \left| \frac{U_M(j\omega)}{C} \right| \quad (6)$$

When calculating the HQSF the effects of control sensitivity must be removed. This is accomplished as follows:

displacement sensing inceptor

$$HQSF = \left| \frac{M}{C}(j\omega) \cdot \frac{1}{K_e} \cdot \frac{1}{Y_c(j\omega)} \cdot Y_{PF}(j\omega) \right| \quad (7)$$

force sensing inceptor

$$HQSF = \left| \frac{M}{C}(j\omega) \cdot \frac{1}{K_e} \cdot \frac{1}{Y_c(j\omega)} \cdot Y_{FS} Y_{PF}(j\omega) \right|$$

Using flight-test handling qualities results, Ref. 8 demonstrated that the HQSF could be used to discriminate among handling qualities levels 1 - 3. Figure 2 shows the HQSF bounds developed in that study. After generating the structural pilot model just described, an aircraft's predicted handling qualities level is determined by the area in Fig. 2 penetrated by the HQSF.

The APC/PIO assessment technique discussed in Ref. 8 utilized the power spectral density (PSD) of the signal u_m in Fig. 1 (with control sensitivity effects removed). The PSD of u_m is defined as

$$\Phi_{u_m u_m}(\omega) = \Phi_{cc}(\omega) \cdot |HQSF|^2 \quad (8)$$

where the PSD of the input $c(t)$ is given by

$$\Phi_{cc}(\omega) = \frac{4^2}{\omega^4 + 4^2} \quad (9)$$

Since the work of Ref. 8 dealt only with linear systems, the particular value of the root-mean-square (RMS) value of $c(t)$ was not important, other than it was held constant at the value implied by Eq. 9. Using flight test results, Ref. 8 demonstrated that $\Phi_{u_m u_m}(\omega)$ could be used to discriminate among PIO rating (PIOR) levels defined as

$$\begin{aligned} 1 &\leq PIOR \leq 2 \\ 2 &< PIOR < 4 \\ PIOR &\geq 4 \end{aligned} \quad (10)$$

The PIOR scale itself is shown in Fig. 3. Figure 4 shows the $\Phi_{u_m u_m}(\omega)$ bounds resulting from the study of Ref. 8. As in the case of the handling qualities levels, an aircraft's predicted PIOR is determined by the area penetrated by $\Phi_{u_m u_m}(\omega)$ when the pilot model is created as described in the preceding.

In Ref. 8, the actual APC/PIO was hypothesized to occur when a "triggering" event with a PIO-prone vehicle ($PIOR \geq 4$) caused the pilot to switch from visual error tracking *with* proprioceptive feedback to error-rate tracking with *no* proprioceptive feedback (switches S_1 and S_2 in Fig. 1 both "up"). A narrow range of gain values K_e was shown to result from the pilot's attempt to maintain control over error-rate while still maintaining stability. The frequency of the APC/PIO was hypothesized to lie between the value corresponding to the peak of $\Phi_{u_m u_m}(\omega)$, and the value of K_e which resulted in neutral closed-loop stability with switches S_1 and S_2 "up".

Analyzing Nonlinear APC/PIO Events

Introduction

Three convenient categories of APC/PIO encounters have been suggested:^{3,4} *Category I* describes events with essentially linear vehicle dynamics and pilot behavior. *Category II* describes events in which fundamental nonlinearities come into play, chiefly those associated with the actuators. *Category III* describes events which fundamentally depend upon nonlinear transitions in either the effective vehicle dynamics or the pilot's behavioral dynamics. The

model-based theory just outlined addresses only Category I events. The research to be described will extend this theory to Category II events, particularly those caused by actuator rate limiting. Extending the theory of Ref. 8 to the case of actuator rate limiting and Category II APC/PIO events should be straightforward. This is because the fundamental metric used to determine APC/PIO susceptibility is simply $\Phi_{u_m u_m}(\omega)$, the PSD of a signal which is easily accessible in a non-real time simulation of the pilot/vehicle system regardless of whether the vehicle description is linear or nonlinear. However it is not just computational convenience which justifies the extension to nonlinear analyses, but rather the *central role* which the spectral characteristics of the signal $u_m(t)$ in the pilot model of Fig. 1 have been demonstrated to play in determining whether the closed-loop pilot/vehicle system is susceptible to APC/PIO's.⁸ Of course, in applying this methodology to nonlinear systems, the linear relationship of Eq. 8 can no longer be used. Also, the nonlinearity introduced by rate limiting means the RMS value of the input can no longer be arbitrary.

Power Spectral Density Calculations

The PSD of the input $c(t)$ was scaled so that a desired RMS control stick displacement resulted when rate limiting was removed. Thus,

$$\Phi_{cc}(\omega)|_{scaled} = \Phi_{cc}(\omega) \cdot \left[\frac{\sigma_{\delta_m}|_{max}}{\sigma_{\delta_m}} \right]^2$$

$$\Phi_{cc}(\omega) = \text{PSD of } c(t) \text{ given by Eq. 9}$$

$$\sigma_{\delta_m}|_{max} = \text{max desired RMS stick displacement}$$

$$\sigma_{\delta_m} = \text{RMS stick displacement when rate limit calculated using } \Phi_{cc}(\omega) \text{ of Eq. 9}$$

(11)

For isometric inceptors, σ_{δ_m} refers to stick force δ_F rather than displacement. As Eq. 11 indicates, $\sigma_{\delta_m}|_{max}$ is chosen as a maximum desirable RMS stick displacement, large enough to vigorously excite the aircraft without being unrealistic. Here,

$$\sigma_{\delta_m}|_{max} = 0.7 \cdot \delta_m|_{max}$$

$$\delta_m|_{max} = \text{maximum physical stick displacement}$$

(12)

In Eq. 12, the *maximum physical stick displacement* refers to half the maximum stick throw. For example, if cockpit stick movement is limited to ± 5 inches, the maximum stick throw is 10 inches and the maximum physical stick displacement is defined as 5 inches. Note that using Eq. 11 and the structural pilot model of Fig. 1 requires thorough documentation of all control and force-feel system characteristics.

The justification for employing Eq. 11 is based upon the following observation: In APC/PIO incidents involving actuator rate limiting, very large cockpit control displacements/forces are typically in evidence, e.g., the traces reported in Ref. 13 for the YF-22. Thus, APC/PIO events involving actuator rate limiting are very likely to be accompanied by large control displacements/forces. Obviously, the choice of $\sigma_{\delta_m}|_{max}$ will influence the amount of actuator rate limiting which will occur in the computer simulation of the pilot/vehicle system. The choice here of 70% of the maximum stick displacement represents a reasonable compromise between choosing a small value which would result in an overly optimistic prediction of APC/PIO susceptibility to rate limiting and choosing a large value which would result in an overly conservative prediction of APC/PIO susceptibility. Assuming the control stick displacement possesses a normal amplitude distribution (with no actuator rate limiting), the $\sigma_{\delta_m}|_{max}$ value of Eq. 12 implies that control stick displacements exceed physical travel approximately 15% of the time. This was felt to be acceptable for the purposes of analysis. Of course, control stick displacement limits could be incorporated in the simulated pilot/vehicle system, but this was eschewed here.

The PSD of $u_m(t)$ is now obtained as

$$\Phi_{u_m u_m}(\omega) = [\Phi_{u_m u_m}(\omega)|_{sim}] \cdot \frac{1}{K_c^2} \cdot \left[\frac{\sigma_{\delta_m}}{\sigma_{\delta_m}|_{max}} \right]^2 \quad (13)$$

where $[\Phi_{u_m u_m}(\omega)|_{sim}]$ represents the PSD obtained

directly from the simulation using the input with PSD given by Eq. 11. Just as in Eqs. 7, the K_c term appearing in Eq. 13 effectively removes control sensitivity effects from the calculation of $\Phi_{u,u_m}(\omega)$. The final term on the right hand side of Eq. 13 is the reciprocal of the final term on the right hand side of Eq. 11. Including this term in Eq. 13 removes scaling effects introduced in Eq. 11 and allows use of the bounds of Fig. 4 to assess APC/PIO susceptibility. Calculating $[\Phi_{u,u_m}(\omega)]_{sim}$ is a fairly straightforward task given the computer-aided control system design and signal analysis packages or "toolboxes" currently available. This will be demonstrated in what follows.

Bracketing the APC/PIO Frequency

A procedure was created for predicting or bracketing the APC/PIO frequency in nonlinear systems experiencing saturation, which parallels that developed for linear systems.⁸ A lower possible APC/PIO frequency, ω_L , is associated with the peak in $\Phi_{u,u_m}(\omega)$. The higher possible APC/PIO frequency is hypothesized to arise from a regressive form of human control behavior in which error-rate tracking occurs with no proprioceptive feedback. In the model of Fig. 1, this control behavior is created by placing switches S_1 and S_2 "up" in the model of Fig. 1. No model parameters are changed, but the appropriate value of K_c must be found. For a vehicle with linear dynamics, this value of K_c was determined by a simple root locus analysis of the system of Fig. 1, i.e., the value of K_c for neutral stability was determined. For a vehicle with nonlinear dynamics this procedure must be modified: The input command $c(t)$ is set to zero and a doublet stick force of brief duration (e.g., 2 s) is injected at the input to the force-feel system in the closed-loop, pilot/vehicle simulation. The amplitude of the force doublet corresponds to a static stick displacement equal to the maximum physical stick displacement in the cockpit. A minimum value of K_c is then found which produces a stable limit cycle of frequency ω_H . Thus, $\omega_L \leq \omega_{PIO} \leq \omega_H$.

The existence a lower and higher possible APC/PIO frequency identified in the manner just described should be common to any configuration which is susceptible to APC/PIO. The reason: The open-loop transfer functions of each pilot/vehicle system will be forced to follow the dictates of Eq. 4, and thus share a common (but not identical) frequency domain

description. The rationale behind bracketing a frequency range in which an APC/PIO frequency might occur is the possibility that an APC/PIO encounter may involve either or both types of pilot behavior (normal or "regressive").

Discussion

It should be noted that the issue of predicting APC/PIO susceptibility attributable to actuator rate saturation has drawn the attention of many researchers.^{4,5,6,7,14,15} These approaches are all potentially useful. In terms of complexity, however, the methodology proposed in Ref. 8 and herein may be the simplest, i.e., no describing function analyses or special optimization procedures are required. Finally, it should be noted that the procedure for determining Category II susceptibility is not limited to systems with a single, isolated nonlinearity. For example, consider the case where vehicle pitch attitude is controlled by canard, elevator and thrust vectoring nozzle, each driven by an actuator with different rate limits. The procedure just outlined can be applied to this vehicle as easily as to one with a single control effector and actuator, albeit with some additional complexity involved in vehicle modeling and simulation. The handling qualities assessment technique using the HQSF was not extended to nonlinear systems herein. However such an extension is possible and could involve calculating the HQSF with existing techniques for determining the Laplace transforms of input-output pairs of nonlinear systems¹⁶. Such a study would provide an interesting avenue for future research. Finally, the methodology discussed here will capture the effects of control sensitivity upon APC/PIO susceptibility only as far as these effects influence the amount of actuator rate saturation that occurs with RMS stick displacements as defined in Eq. 12.

Examples: Configurations from the LAHOS Data Base

Each of the examples that follow requires appropriate pilot models as described in the previous section and summarized in Eqs. 1-5. Selecting model parameters requires no guesswork by the analyst, with the possible exception of the value of "a" implied by Eq. 2. Selecting a suitable "a" via Eqs. 4 and 5 may require some engineering judgement. This is particularly true when higher-order aircraft models are employed. For example, consider the case when Eq. 5 indicates Y_{PF} requires the form $K/(s+a)$ but no simple isolated pole exists in the vehicle transfer function.

Closing the proprioceptive loop places the $(s+a)$ term in the numerator of the pilot transfer function, but there is no matching term in the denominator, and therefore dynamic cancellation is incomplete. In such cases, selection of "a" should be dictated by the creation of the largest possible gain and phase margins commensurate with the dictates of Eq. 5. The forms of Y_{PF} used herein will be presented at appropriate points in the discussion.

Although actuator rate saturation or rate limiting has been implicated in a number of recent and important APC/PIO events, e.g. the YF-22^{3,13}, the JAS-39 Gripen^{3,17} and the C-17^{3,5}, a data base for actuator rate-limiting comparable to other handling qualities flight-test studies (e.g., Refs. 18 and 19) has yet to be established. For this reason, rate limiting has been introduced analytically in the nonlinear configurations to be analyzed, much as was done in Ref. 7. The flight-test configurations to be modified were taken from the venerable LAHOS data base. The basic configurations to be analyzed are shown in Table 1. In simulating the behavior of a rate-limited actuator in the examples to follow, a rate limiting element was introduced after the linear, second-order actuator of Table 1. If the input to this element exceeded the rate limit of the actuator, the element's output became rate limited and remained so until input and output were equal. For the examples to be discussed, $\Phi_{u,u_n}(\omega)$ was obtained from a 240 s simulation run with an input PSD given by Eq. 11. The sampling frequency was 25 Hz and the resulting raw PSD was smoothed by replacing each point ($\Phi_{u,u_n}(\omega)$) by the average of 20 neighboring points (0.19 rad/s to either side of the frequency point in question). This smoothing operation is important, as it produces a more continuous PSD from single simulation runs.

LAHOS Config. 4-7 Configuration 4-7 in the LAHOS data base was rated as having satisfactory handling qualities.¹⁹ The average Cooper-Harper rating in flight test was 3.0 (level 1) and the average PIOR was 1. In the pilot model for this configuration,

$$Y_{PF} = \frac{K}{s+3} \quad (14)$$

The resulting HQSF and $\Phi_{u,u_n}(\omega)$ are shown in Figs 5 and 6 where the HQSF was obtained from Eq. 7. Since

nonlinearities have yet to be introduced, $\Phi_{u,u_n}(\omega)$ could have been obtained analytically from Eq. 8. However, it was obtained from a simulation of the pilot/vehicle system using Eq. 13 as just described. As Figs. 5 and 6 show, the HQSF and $\Phi_{u,u_n}(\omega)$ are each below the level 1 and $1 \leq \text{PIOR} \leq 2$ bounds of Figs. 2 and 4, respectively.

LAHOS Config. 4-7 with Actuator Rate Limiting An elevator actuator rate limit of 25 deg/s was implemented in the simulation. The Y_{PF} is still given by Eq. 14. Herein, $\sigma_{\delta}|_{\max}$ was chosen as 3.5 inches, or 70% of the physical limits of stick displacement (± 5 inches in the test aircraft). No HQSF is obtained for the nonlinear case, since the transfer function in question, i.e., Eq. 7, is no longer defined. Figure 7 shows $\Phi_{u,u_n}(\omega)$ for Config. 4-7 with actuator rate limiting. The maximum value of $\Phi_{u,u_n}(\omega)$ now occurs in the area predicting $2 < \text{PIOR} < 4$.

LAHOS Config. 4-7 With Time Delay To degrade the linear vehicle handling qualities from those of the nominal Config. 4-7, a time delay of 0.2 s was introduced into the stick filter as indicated in Table 1. This is a contrived example, as no time delay was introduced in the flight test of Config. 4-7. Figures 5 and 6 also show the HQSF and $\Phi_{u,u_n}(\omega)$ which was obtained for this configuration. The Y_{PF} given by Eq. 14 remains unchanged. Note that the modeling procedure now indicates level 3 handling qualities and $2 < \text{PIOR} < 4$ should be expected with this vehicle. As opposed to the nominal Config. 4-7 with actuator rate limiting present, the $\Phi_{u,u_n}(\omega)$ for this configuration is nearly in the $\text{PIOR} \geq 4$ region, indicating a Category I PIO is likely.

LAHOS Config. 4-7 With Time Delay and Actuator Rate Limiting Figure 7 shows $\Phi_{u,u_n}(\omega)$ for Config 4-7 with time delay and actuator rate limiting. Note that the introduction of a rate-limited actuator has taken the vehicle from a predicted $2 < \text{PIOR} < 4$ to a prediction of $\text{PIOR} \geq 4$. This indicates a Category II PIO should definitely be expected. The procedure for bracketing the APC/PIO frequency outlined previously was invoked. Figure 7 indicates a peak in $\Phi_{u,u_n}(\omega)$ at 1.93 rad/s. Figure 8 shows the limit cycle

in control stick displacement associated with the lowest value of K_t which produced such a stable oscillation with no proprioceptive feedback (switches S_1 and S_2 in Fig. 1 "up"). Larger values of K_t produced limit cycles with larger amplitudes but lower frequencies than that of Fig. 8. Note that initial stick displacements are well beyond the ± 5 inch physical cockpit limitation. This, result is of little consequence here since the purpose of the injected doublet is merely to excite the system sufficiently to express the limit cycle. Figure 8 shows the resulting limit cycle amplitude is approximately 2 inches with a frequency of 3.27 rad/s. Thus APC/PIO frequency can be bracketed by

$$1.93 \text{ rad/s} \leq \omega_{PIO} \leq 3.27 \text{ rad/s} \quad (15)$$

The large difference between these frequencies (nearly a factor of 2) deserves some comment. If one considers Config. 4-7 of Fig. 7 (with delay but *without* rate limiting) to be near enough to the $PIOR \geq 4$ boundary to be considered definitely APC/PIO prone, then the techniques of Ref. 8 bracket the APC/PIO frequency as

$$2.5 \leq \omega_{PIO} \leq 3.41 \text{ rad/s} \quad (16)$$

with a considerably smaller range involved (a factor of 1.4). Thus, the larger range of Eq. 15 is attributable to the fundamental nonlinearity involved, and not the methodology.

LAHOS Config. 4-4 In contrast to Config. 4-7, LAHOS Config. 4-4 exhibited poor handling qualities and less than ideal PIOR's in flight test. The average Cooper-Harper rating given by evaluation pilots was 6.5, and the average PIOR was 2.67. Since the handling qualities for this configuration were poor, *ab initio*, adding a time delay to artificially degrade vehicle handling qualities as was done with Config. 4-7, was unnecessary. In the pilot model for this configuration,

$$Y_{PF} = \frac{K}{s+2} \quad (17)$$

Figures 9 and 10 show the HQSF and $\Phi_{u,u_m}(\omega)$ for this configuration which place the aircraft at the border between level 2 and level 3 handling qualities, and $2 < PIOR < 4$. It should be noted that the poor handling qualities and relatively poor PIOR's of Config. 4-4 were attributable to a first-order filter with a low break frequency of 2.0 rad/s placed between the control stick

and the elevator actuator. Configuration 4-7 also possessed a stick filter, however it was a second-order filter with an undamped natural frequency of 12.0 rad/s and a damping ratio of 0.7. As Table 1 indicates, the bare-airframe dynamics for Configs. 4-4 and 4-7 were identical.

LAHOS Config. 4-4 with Actuator Rate Limiting Actuator rate limiting of 25 deg/s was implemented in a computer simulation of the pilot/vehicle system with the input PSD given by Eq. 11. The Y_{PF} given by Eq. 16 remains unchanged. The $\Phi_{u,u_m}(\omega)$ for Config. 4-4 with actuator rate limiting is shown in Fig. 10. As opposed to the results for Config. 4-7, the presence of actuator rate limiting in Config. 4-4 is not predicted to increase APC/PIO susceptibility. While $\Phi_{u,u_m}(\omega)$ still penetrates the area associated with $2 < PIOR < 4$, the peak value of $\Phi_{u,u_m}(\omega)$ is considerably smaller than that for Config. 4-4 without limiting. This result is attributable to the aforementioned first-order filter which reduces the amount of actuator rate limiting occurring with large stick inputs as compared to that occurring with Config. 4-7. This result does not exonerate the vehicle from PIO susceptibility, since rather poor linear PIO characteristics have been predicted. However, a progression from a Category I to Category II APC/PIO, is unlikely. Also, the stick filter is not a cure for the PIO problem since it is this filter which degrades the handling qualities of Config. 4-4 as compared to Config. 4-7.

LAHOS Config. 4-7 Without Delay and With Actuator Rate Limiting of Different Magnitudes As a final example, Config. 4-7 was simulated without time delay but using four different levels of actuator rate limiting: no rate limiting, 75 deg/s, 50 deg/s, and 25 deg/s. Figure 11 shows the $\Phi_{u,u_m}(\omega)$ which resulted. It is interesting to note that there is no APC/PIO susceptibility predicted for the 75 deg/s case, and the 50 deg/s case involves only a small violation of the bound associated with $1 \leq PIOR \leq 2$. This example is important as it represents the type of problem likely to be addressed with the proposed methodology, i.e., assessing the effects of actuator rate limiting on an aircraft which exhibits satisfactory handling qualities in the absence of such limiting.

Discussion

The eight examples of the preceding section were intended to demonstrate the proposed methodology for predicting APC/PIO susceptibility, with emphasis upon Category II events. It should be emphasized that, in the preceding examples, the excellent correlation obtained between model predictions and flight test for Configs. 4-7 and 4-4 (no delay, no rate limiting) should be expected, as these configurations were among those used to establish the HQSF and PIOR bounds of Figs. 2 and 4.⁸ Obviously, it is desirable, if not essential, to apply the methodology to other cases involving actuator rate limiting for which flight-test information is available. However, as mentioned in the preceding, almost no data base exists for situations involving such nonlinear behavior. And where data do exist, company proprietary restrictions often prevent disseminating sufficiently detailed information to apply this or competing methodology. However, in the absence of such a data base, the methodology proposed herein may still offer a tractable means to assess APC/PIO susceptibility. This is especially true if the goal is simply to minimize this susceptibility.

Analytical Assessment of Category I and II APC/PIO Susceptibility

A formal procedure for assessing APC/PIO susceptibility can now be proposed. Given descriptions of the vehicle, actuation, and force-feel system dynamics, (including system gains/sensitivities) a pilot model is created using the guidelines outlined previously. The susceptibility of an aircraft to Category I or Category II APC/PIO events is assessed as follows:

Category I The linear system is analyzed first to determine the likelihood of linear APC/PIO events. If $\Phi_{u,u_m}(\omega)$ obtained from Eq. 8 using the command input of Eq. 9 exceeds the bound of Fig. 4 associated with $2 < \text{PIOR} < 4$ in Fig. 4, an improvement in the flight control system may be warranted. If $\Phi_{u,u_m}(\omega)$ exceeds the bound associated with $\text{PIOR} \geq 4$, a linear (Category I) APC/PIO should be expected. The frequency of the APC/PIO is predicted to fall the frequency of the peak value of $\Phi_{u,u_m}(\omega)$ and the frequency associated with the value of K_t which yields neutral stability when switches S_1 and S_2 in the model of Fig. 1 are "up". In addition to predicting the likelihood of APC/PIO encounter, the methodology of Ref. 8 also allows the prediction of handling qualities levels using the HQSF and the bounds of Fig. 2.

If the aircraft is exonerated from susceptibility to Category I APC/PIO events, susceptibility to Category II events is examined next. The pilot model developed for the Category I analysis remains unchanged.

Category II Using the command input with PSD given by Eq. 11, a computer simulation of the pilot/vehicle system is undertaken which includes any actuator rate limits. As in the case of the linear system, the likelihood of nonlinear APC/PIO events is interpreted using $\Phi_{u,u_m}(\omega)$ and the bounds of Fig. 4. If $\Phi_{u,u_m}(\omega)$ obtained from Eq. 13 exceeds the bounds associated with $\text{PIOR} \geq 4$, a nonlinear (Category II) APC/PIO should be expected. The frequency of the predicted APC/PIO can be bracketed as follows: The lower frequency is that associated with the peak in $\Phi_{u,u_m}(\omega)$. The higher frequency is obtained through a second simulation. Switches S_1 and S_2 in the model of Fig. 1 are "up". A doublet force disturbance of 2 s duration is injected at the input to the force-feel system in a closed-loop simulation of the pilot/vehicle system. The amplitude of the force doublet corresponds to a static stick displacement equal to the maximum physical stick displacement in the cockpit. The higher APC/PIO frequency is the frequency of the limit stable limit cycle associated with the smallest value of K_t which yields a stable limit cycle.

Conclusions

One of the recommendations which addressed criteria for APC/PIO assessment in Ref. 3 reads as follows:

"Research to develop design assessment criteria and analysis tools should focus on Category II and III PIO's.....This research should combine experiments with the development of effective analytical analysis methods capable of rationalizing and emulating the experimental results" (emphasis added).

The research summarized herein has been an attempt to develop such analysis methods. In particular, an existing technique for assessing the APC/PIO susceptibility of aircraft described by linear dynamics has been extended to aircraft described by nonlinear dynamics. As exercised here, the nonlinearity was actuator rate limiting which can serve as a catalyst for Category II APC/PIO events. The extended technique relies upon calculating the power